244–254 *Nucleic Acids Research, 2017, Vol. 45, No. 1* *Published online 7 October 2016*
doi: 10.1093/nar/gkw904

ATM induces MacroD2 nuclear export upon DNA damage

Barbara Golia[1], Giuliana Katharina Moeller[1], Gytis Jankevicius[1], Andreas Schmidt[2], Anna Hegele[1], Julia Preißer[1], Mai Ly Tran[1], Axel Imhof[2] and Gyula Timinszky[1,*]

[1]Department of Physiological Chemistry, Biomedical Center, Ludwig-Maximilians-Universität München, Planegg-Martinsried 82152, Germany and [2]Zentrallabor für Proteinanalytik (Protein Analysis Unit), Ludwig-Maximilians-Universität München, Planegg-Martinsried 82152, Germany

Received June 10, 2016; Revised September 08, 2016; Accepted October 04, 2016

ABSTRACT

ADP-ribosylation is a dynamic post-translation modification that regulates the early phase of various DNA repair pathways by recruiting repair factors to chromatin. ADP-ribosylation levels are defined by the activities of specific transferases and hydrolases. However, except for the transferase PARP1/ARDT1 little is known about regulation of these enzymes. We found that MacroD2, a mono-ADP-ribosylhydrolase, is exported from the nucleus upon DNA damage, and that this nuclear export is induced by ATM activity. We show that the export is dependent on the phosphorylation of two SQ/TQ motifs, suggesting a novel direct interaction between ATM and ADP-ribosylation. Lastly, we show that MacroD2 nuclear export temporally restricts its recruitment to DNA lesions, which may decrease the net ADP-ribosylhydrolase activity at the site of DNA damage. Together, our results identify a novel feedback regulation between two crucial DNA damage-induced signaling pathways: ADP-ribosylation and ATM activation.

INTRODUCTION

ADP-ribosylation is a reversible post-translational modification implicated in the regulation of several cellular processes, such as genomic stability, chromatin structure, transcription and RNA metabolism (1–3). Proteins are most often ADP-ribosylated by poly(ADP-ribose) polymerases (PARPs), also known as ADP-ribosyltransferase diphtheria toxin-like proteins (ARTDs), which transfer an ADP-ribose moiety from nicotinamide adenine dinucleotide (NAD^+) onto target proteins, typically in response to various forms of cellular stress (4,5). The best studied members of the PARP family—PARP1, PARP2, PARP5a (TNKS1) and PARP5b (TNKS2) – generate poly(ADP-ribose) (PAR) (3). The remaining PARP members can only transfer a single mono(ADP-ribose) (MAR) onto target proteins, with the exception of two—PARP9 and PARP13—that are enzymatically inactive. Besides the MARylating PARPs, the deacetylase sirtuins SIRT2, SIRT4 and SIRT6 were also reported to MARylate target proteins (6–8).

The regulation of the ADP-ribosylating enzymes remains poorly understood, and previous studies are essentially limited to PARP1. PARP1 enzymatic activity is increased by SET7/9-dependent methylation (9), SIRT6-induced MARylation (10) and cyclin-dependent kinase 2 (CDK2)-dependent phosphorylation (11). But the best known enhancers of PARP1 activity are DNA lesions (2). During the DNA damage response, PARP1 is important for the repair of both single- and double-strand breaks (DSBs). DNA damage-induced activation of many pathways also provides intriguing examples of signal integration involving ADP-ribosylation. During DSB repair, an interaction between PARP1 and ataxia-telangiectasia-mutated (ATM) kinase, a member of the PI3K-like kinase family, has been reported. When cells undergo DNA damage, PARP1 is phosphorylated at multiple residues, some of which are targets of ATM (12–14). Additionally, since ATM contains two PAR-binding motifs, PAR formation at DNA lesions induces recruitment of ATM (15,16).

The number of enzymes known to reverse ADP-ribosylation is much smaller. PAR glycohydrolase (PARG) and ADP-ribosylhydrolase 3 (ARH3) catalyze the degradation of PAR by hydrolyzing the O-glycosidic ribose-ribose bonds (3). However, they cannot remove the most proximal mono(ADP-ribose). MacroD1, MacroD2 and TARG1, three human enzymes with enzymatic macrodomain, were shown to reverse protein MARylation (17–19). The *in vivo* functions and regulation of these macrodomain hydrolases remain essentially unknown. MacroD1 has an N-terminal mitochondrial targeting sequence and localizes within mitochondria, suggesting that its substrates are mitochondrial as well. Both TARG1 and MacroD2 are present in the nucleus and the cytoplasm (19,20), although they differ in the

*To whom correspondence should be addressed. Tel: +49 89 2180 77100; Fax: +49 89 2180 77093; Email: gyula.timinszky@med.uni-muenchen.de
Present address: Gytis Jankevicius, Sir William Dunn School of Pathology, Oxford OX1 3RE, UK.

protein sequence. The TARG1 sequence consists only of a macrodomain, but MacroD2 is twice the size of TARG1, containing a C-terminal region as long as the macrodomain itself. Although the exact molecular functions of MacroD2 are unknown, it has been associated with cancer and neurological disorders (21–27).

Published studies have so far focused only on the MacroD2 macrodomain, showing its recruitment to DNA lesions (17,18). Since both PARG and TARG1 deficiencies are associated with neurodegeneration and DNA repair defects (19,28), the MacroD2 association with cancer and neurological disorders prompted us to study the behavior of full-length MacroD2 upon DNA damage.

MATERIALS AND METHODS

Reagents and antibodies

DMSO (D2438—Sigma); etoposide (E1383—Sigma-Aldrich); PARP inhibitor Olaparib (AZD2281—Selleckchem); ATM kinase inhibitor (KU55933—Selleckchem); ATR kinase inhibitor (VE-821—Selleckchem); DNA-PK kinase inhibitor (NU7441—Selleckchem); NAMPT inhibitor (FK-866—Sigma-Aldrich); (^{32}P)γATP (FP-301—Hartmann Analytic); GFP-trap (gta—Chromotek); bisBenzimide H 33342 trihydrocloride (Hoechst) (Sigma).

Anti-GAPDH (rat monoclonal #5C4 from Dr Kremmer of Helmholtz Zentrum Munich); anti-ATM [Y170] (ab32420, rabbit monoclonal, Abcam); Alexa-488 goat anti-rabbit (Invitrogen); goat anti-rabbit IgG-HRP conjugated (BIO-RAD); anti-rat IgG-HRP conjugated (Jackson ImmunoResearch). Anti-MacroD2 (rabbit polyclonal #494-7) was generated by in-house facility, by injecting rabbits with the purified V5-tagged MacroD2 macrodomain protein described in (17). Serum was affinity-purified by coupling MacroD2 macrodomain protein to CNBr Sepharose using standard protocol.

Plasmids

Mammalian expression constructs of wild-type MacroD2 macrodomain was described previously (29). The mammalian expression construct of wild-type MacroD2 full length (aa 1–448) was obtained by PCR from human testis cDNA library (Clontech) and inserted into the pmEGFP-C1 vector by using BglII and EcoRI restriction sites. Wild-type MacroD2 C-terminal domain (aa236–448) and MacroD2 shorter fragments (aa382–418), (aa402–418) and (aa410–418) were generated by cloning of the PCR-amplified corresponding sequence from the above mentioned full-length construct into the pmEGFP-C1 vector by using BglII and EcoRI restriction sites. The following mutants were generated from MacroD2 full-length construct by using QuikChange site-directed mutagenesis (Stratagene) according to the manufacturer's protocol: S276 345 415 426A; S345 415 426A; S276 415 426A; S276 345 426A; S276 345 415A. The following mutants were generated from MacroD2 (aa382–418): S415A; Q416A. The following mutants were generated from MacroD2 (aa336–372): S345A; Q346A. All constructs were sequence verified.

Bacterial expression constructs: a pETM-CN vector-based His6-TEV-mEGFP-tagged human MacroD2 C-terminal domain (aa236-448) construct was generated by amplifying the desired fragment from the above mentioned pmEGFP-C1-MacroD2 C-terminal region and inserting it in the vector with BamHI and XbaI enzymes. mEGFP-tagged MacroD2 (aa382–418) was generated in two versions: pETM-CN-His6-TEV and pGEX-6P1-GST, generated by inserting the same sequence amplified from pmEGFP-MacroD2 (aa382–418) respectively with BamHI–XbaI and BamHI–EcoRI restriction enzymes. Corresponding point mutants of the Hi6-version were generated through the QuikChange site-directed mutagenesis (Stratagene) protocol: D410A, V411E, E412A, M413A, N414A, S415A and Q416A. All constructs were sequence verified.

Cell culture, transfection and siRNA treatment

Human U2OS cell lines stably expressing mYFP–MacroD2 full length+mCherry-H2B or mEGFP-MacroD2 C-terminal domain (aa236-448)+mCherryH2B were grown in DMEM (Sigma) containing 10% (v/v) FBS (Gibco), 2 mM L-glutamine (Sigma), 100 U ml^{-1} penicillin, 100 μg ml^{-1} streptomycin (Sigma) and 200 μg ml^{-1} G418 (Gibco). For transient transfections, a human HeLa Kyoto cell line stably expressing mCherry-H2B was used. DNA transfection was performed by means of Xfect (Clontech) according to the manufacturer's recommendations. For siRNA-mediated MacroD2 and ATM depletion, Negative Control #2, s44380 and s1708 Silencer Select siRNA oligonucleotides (Ambion) were used in combination with Lipofectamine RNAiMAX (ThermoFisher) according to the manufacturer's protocol. Cells were tested on the third day of siRNA treatment.

Live-cell imaging, pulsed-laser microirradiation and image analysis

Cells were plated in borosilicate 8-well Lab-Tek chambered cover glasses (ThermoScientific) or in black cycloolefin-covered 96-well plates (Greiner). During the experiments, cells were kept at 37°C in Phenol Red-free Leibovitz's, a CO_2-independent imaging medium (Sigma) supplemented with 10% (v/v) FBS (Gibco), 2 mM L-glutamine (Sigma), 100 U ml^{-1} penicillin and 100 μg ml^{-1} streptomycin (Sigma). When indicated, inhibitors were added to the culture medium 30 min before imaging, with the exception of FK-866, whose incubation started 16 h before imaging. Imaging was performed on a Zeiss AxioObserver Z1 confocal spinning-disk microscope equipped with an AxioCam HRm CCD camera (Zeiss) through a Zeiss C-Apochromat 40×/1.2 water-immersion objective or a Zeiss Plan-Apochromat 20×/0.8 lens. For laser microirradiation, we used a 355-nmwavelength, diode-pumped, solid-state, pulsed laser (DPSL-355/14, Rapp OptoElectronics). DNA damage was induced by focusing the laser to a point or a line in the nucleus or by adding etoposide for a final concentration of 10 μM. Cells were imaged every 10 seconds or 1 minute for 30 min or every 5 min for 100 min.

The time-lapse and the immunofluorescence images were analysed with CellProfiler 2.0 (30). The mCherry-H2B or

Hoechst images were used for the segmentation of the nucleus. To quantify protein export upon treatment, background was first subtracted and the ratio of nuclear intensity over cytoplasmic intensity of GFP-MacroD2 was calculated. For the time-lapse images, the ratio of each time point was normalised to the first time point. To quantify the amount of protein recruited to DNA damage site, we registered the cells with MultiStackReg plugin (http://bradbusse.net/sciencedownloads.html) in Fiji (http://fiji.sc/Fiji), subtracted the background and normalised the mean intensity of recruitment area over the mean intensity of the total cell. Then, we normalised the ratio at each time point to the intensity of the initial time point. To compare nuclear signal depletion with cytoplasmic signal increase, the analysis was as described before, but comparing nuclear mean intensity over cell mean intensity versus cytoplasm mean intensity over cell mean intensity. Igor Pro (WaveMetrics) or R were used for analysing and plotting the data.

Immunocytochemistry

U2OS cells were plated in borosilicate 8-well Lab-Tek chambered cover glasses (ThermoScientific). Treatment with etoposide 10 μM was performed for one hour. Cells were then fixed and permeabilised with Methanol/Acetone 1:1 solution for 10 min at –20°C. Blocking was performed with PBS–Tween 0.1% with BSA 5%. Cells were incubated with the antibody anti-MacroD2 antibody (1:500), diluted in PBS-Tween 0.1%–BSA 3%, for 1 h at room temperature. Incubation with Alexa-488-conjugated antibody (1:500) was performed for 1 h at room temperature. Lastly, cells were incubated with Hoechst 33342 (Sigma) at 200 ng ml^{-1} final concentration for 10 minutes.

Protein expression and purification

Protein expression constructs were expressed in *Escherichia coli* Rosetta(DE3)pLysS cells at 18°C for 16 h after 0.2 mM IPTG induction. Cell pellets were snap-frozen in liquid nitrogen and stored at −80°C. For histidine-tagged protein purification, the thawed pellet was resuspended in a lysis/wash buffer (50 mM Tris–Cl, pH 7.5, 0.5 M NaCl, 20 mM imidazole, 1 mM DDT and protease inhibitor cocktail (Roche)). Lysates were sonicated for 20 × 18 s at medium setting (Branson) until the lysate was not viscous and centrifuged for 45 min at ∼45 000 g at 4°C. The supernatant was exposed to a column with Ni-NTA agarose (Qiagen), washed three times with 30 ml wash buffer and eluted with wash buffer containing 500 mM imidazole. The proteins were dialyzed in storage buffer (25 mM Tris–Cl, pH 7.5, 0.25 M NaCl, 1 mM DTT) with PD-10 columns (17-0851-01; GE-Healthcare). Peak fractions were confirmed by SDS-PAGE and Coomassie staining. Concentrations were determined by Bradford assay (Biorad). For GST-tagged protein purification, the procedure was as above, with the exception that glutathione Sepharose 4 Fast Flow (GE-Healthcare) and 20 mM reduced-glutathione elution buffer (GE Healthcare) were used.

Immunoblotting

RIPA buffer (50 mM Tris–Cl, pH 7.5, 0.15 M NaCl, 0.1% sodium deoxycholate, 1 mM EDTA, 1% NP-40) was used to obtain whole cell lysate, whose concentration were determined via a Bradford assay on strongly diluted samples. Proteins were resolved on 12% or 6% + 12% SDS-PAGE and transferred onto nitrocellulose membrane (Whatman Protran). The membrane was blocked in PBS-Tween 0.05% buffer supplemented with 5% non-fat milk. Proteins were detected with the appropriate primary antibodies and secondary antibodies coupled to horseradish peroxidase. Detection was performed with Immobilon Western Blotting detection reagent (GE Healthcare).

Phospho-peptide enrichment upon DNA damage

Human U2OS cell lines stably expressing mYFP–MacroD2 full length+mCherry-H2B were treated with etoposide 5 μM or DMSO for 1 h. Cells were then collected on ice and treated with lysis buffer (25 mM Tris–Cl, pH 7.5, 0.15 M NaCl, 0.5% NP-40, 10 mM NaF, 1 mM Na_3VO_4, phosphatase inhibitor cocktail (PhosSTOP – Roche) and protease inhibitor cocktail (Roche)). Lysates were than diluted 1:5 with dilution buffer (as lysis buffer, but with 0.01% NP-40). After vigorous centrifugation, the supernatant was collected and the input was kept. Proper amounts of GFP-trap (Chromotek), previously washed with lysis:dilution buffer, were incubated with the supernatant for 1 h at 4°C with agitation. The beads were then washed two times with lysis:dilution buffer and once with washing buffer (as dilution buffer, but with 500 mM NaCl). Beads were then kept in storage buffer (PBS, 100 mM NaF, 10 mM Na_3VO_4, phosphatase inhibitor cocktail (PhosSTOP – Roche) and protease inhibitor cocktail (Roche)).

Proteomics sample preparation and data analysis

Proteins bound to beads were treated with 5 mM DTT to reduce disulfide bonds and subsequently alkylated using 20 mM iodoacetamide. Proteins were cleaved with AspN for 12 h at 25°C. Following proteolytic digest, peptide mixtures were desalted on reverse-phase C18 stage tips. 90% of the peptide mixture was mixed with 2 M glycolic acid for phosphopeptide enrichment on TiO_2 as described in (31), then loaded onto the prepared TiO_2 resin (Glygen). Eluted phosphopeptide mixtures and peptide mixtures were separated on an Ultimate 3000 nano-RP-HPLC coupled to an LTQ-Orbitrap mass spectrometer (both Thermo-Fisher). The mass spectrometer was operated in data-dependent acquisition mode with one survey scan for precursor mass detection and up to six MS/MS experiments per cycle. CID-MS/MS experiments were conducted with multi-stage activation for neutral loss masses of 32.7, 49 and 98. For MS acquisition, monoisotopic precursor selection and dynamic exclusion for 30 s were enabled.

Raw data were searched with MaxQuant versus 1.5 against a human protein database (Uniprot, May 2015) and an in-house target database containing common target protein and contaminants. All phosphopeptide hits for MacroD2 were manually curated. To quantify the phosphorylation, peak areas for the most abundant charged states

for unmodified peptides and phosphopeptides of the target protein were extracted from the raw data of the peptide mixture before phosphopeptide enrichment and $\log_2$ normalized. Signal strength of unmodified peptides was used for normalization of the protein amount between control and treatment experiments of each biological replicate. Proteomics data are available in ProteomeXchange and Pride (32) with the dataset identifier PXD003712.

Radioactivity kinase assay

Human U2OS cell lines stably expressing mYFP–MacroD2 full length, mEGFP-MacroD2 macrodomain or mEGFP-MacroD2 C-terminal domain were collected on ice. For the kinase assay on purified MacroD2 fragments: His-mEGFP-MacroD2 C-terminal (aa236-448) fragment (200 pmol per sample); GST-mEGFP-tagged MacroD2 (aa382-418) fragment and His-mEGFP-tagged MacroD2 (aa382-418) fragments (wild-type and mutants) (1 nmol per sample); human HEK293 T-REx cells (ThermoFisher) were collected on ice.

Cells were resuspended in lysis buffer (25 mM Tris–Cl, pH 7.5, 0.15 M NaCl, 0.5% NP-40, phosphatase inhibitor cocktail (PhosSTOP – Roche) and protease inhibitor cocktail (Roche)), then incubated on ice for 30 min while mechanically lysed by syringe. Where appropriate, KU55933 at the final concentration of 10 μM was added. The cell lysate was then supplemented with 250 U benzonase nuclease (Sigma), $MgCl_2$ to a final concentration of 4 mM and 2 μCi (^{32}P)γATP (FP-301 – Hartmann Analytic). The lysate was incubated at 37°C for 40 min. It was then cleared from the chromatin with a maximum speed centrifugation, diluted by 1:5 with dilution buffer (as lysis buffer, but with 0.01% NP-40) and the input was kept. Proper amounts of GFP-trap (Chromotek), previously washed with lysis:dilution buffer, were incubated with the supernatant for 1 h at 4°C with agitation. The beads were then washed two times with lysis:dilution buffer and once with washing buffer (as dilution buffer, but with 500 mM NaCl). Input and beads were boiled for 10 min at 95°C in equal amounts of 2× loading buffer (125 mM Tris pH 6.8, 20% glycerol, 2.5% SDS, 0.01% bromophenol blue). Samples were separated on 1 mm Bis–Tris, 4–12% acrylamide NuPAGE gel according to the manufacturer's protocol (Invitrogen).

For the U2OS cell lines experiment, the gel was stained with Coomassie G-250 and dried. Gels were then imaged (ImageScanner III – GE Healthcare) and exposed to imaging plates (Fuji Film). For the kinase assay on MacroD2 fragments, the gel was stained and imaged (ImageScanner III – GE Healthcare). Quantification for the kinase assay on purified mutant MacroD2 fragments was performed by defining the intensity of every band. Each His-construct intensity was subtracted of the residual intensity in the His-S415A mutant, whose radioactivity signal is generated by the degradation of the upper wild-type-containing band, when GST-tag is lost. Then, the adjusted His-construct intensities were normalised to the GST-construct intensity of the same lane, normalised to the wild-type/wild-type ratio and averaged.

RESULTS

MacroD2 exports from the nucleus upon DNA damage

We previously identified MacroD2 as a mono-ADP-ribosylhydrolase and showed that its macrodomain recruits to DNA lesion induced by laser microirradiation (17,18). To further study the role of MacroD2 upon DNA damage, we transfected U2OS cells with mEGFP-tagged full-length MacroD2. The levels of GFP-tagged MacroD2 decreased in the nucleus upon UV microirradiation-induced DNA damage, a behavior not observed for mEGFP alone (Supplementary Figure S1A and B). The decrease in nuclear fluorescence was accompanied by fluorescence increase in the cytoplasm, consistent with the net export of MacroD2 from the nucleus to the cytoplasm upon DNA damage (Supplementary Figure S1C).

The speed of MacroD2 nuclear export was proportional to the amount of DNA damage induced by laser microirradiation (Figure 1A and B). We also confirmed MacroD2 export in cells treated with the topoisomerase II poison etoposide, which induces DNA double-strand breaks (Figure 1C and D). We next tested if the endogenous MacroD2 is exported from the nucleus. We developed an in-house anti-MacroD2 antibody that recognizes endogenous MacroD2 at 70 kDa in U2OS whole cell lysates (Supplementary Figure S1D). In U2OS cells, endogenous MacroD2 shows nuclear depletion upon DNA damage induced with 1 hour of etoposide treatment, as revealed by immunofluorescence microscopy (Figure 1E and F).

As DNA damage-induced nuclear export was not observed for TARG1 (19), we hypothesized that the unique MacroD2 C-terminal region could be involved in MacroD2 localization. Protein secondary structure prediction suggests that the C-terminal domain to be disordered (Figure 1G; (33)). Since intrinsic disordered regions (IDRs) frequently play important regulatory roles by providing binding sites for interacting proteins or through regulation by post-translational modifications, we considered it an interesting feature of MacroD2 to investigate further. We compared the export of MacroD2 full-length versus the macrodomain or the C-terminal fragment in HeLa cells treated with etoposide (Supplementary Figure S1E). Both the full-length and the C-terminal IDR constructs exported, the macrodomain alone did not, identifying the C-terminal IDR of MacroD2 as a regulatory region mediating the DNA damage-induced export of MacroD2.

ATM kinase activity induces MacroD2 nuclear export

By removing mono-ADP-ribose from target proteins, MacroD2 regulates ADP-ribosylation (17,18), a post-translational modification that is quickly produced upon DNA damage and is linked to both single- and double-strand break repair pathways (1,2). We first tested if PARylation affected the nuclear export of MacroD2. We inhibited PARylation by treating cells with Olaparib, a potent inhibitor of PARP1, PARP2, PARP3 and PARP4. While the treatment abolished the recruitment of MacroD2 to the site of DNA damage, its nuclear export remained unchanged (Figure 2A and B). Thus, PARylation does not trigger MacroD2 nuclear export and the macrodomain is

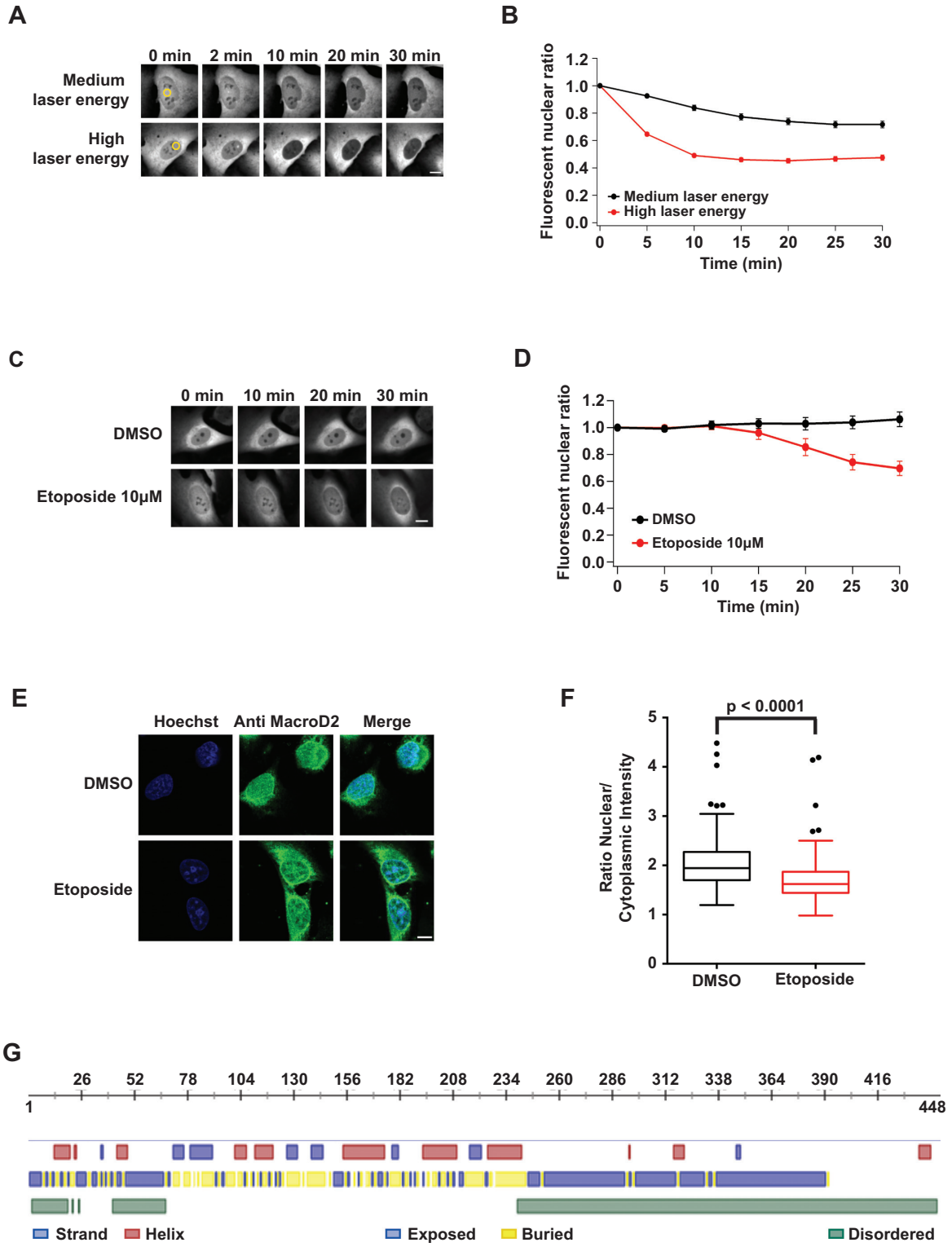

Figure 1. MacroD2 exports from the nucleus upon DNA damage. (**A**) Microirradiation live-cell microscopy of U2OS cells stably expressing the mEGFP-MacroD2 full–length construct. Arbitrary medium and high laser energy values are used to induce different amounts of damage to the cell. Scale bar, 10 μm. (**B**) Quantification of *A*. (**C**) Live-cell imaging of U2OS-mEGFP-MacroD2 full-length cells treated either with etoposide 10 μM or DMSO. Scale bar, 10 μm. (**D**) Quantification of *C*. (**E**) Immunocytochemistry with anti-MacroD2 antibody on cells treated either with etoposide 10 μM or DMSO. Scale bar, 10 μm. (**F**) Quantification of *E* in three independent experiments. Statistics performed with unpaired non-parametrical Kolmogorov-Smirnov test. (**G**) Predictions of MacroD2 secondary structure. Sequence of MacroD2 Isoform 1 of Uniprot was analysed with the online software PredictProtein (33). The first line shows prediction for the presence of helices or strands of beta sheets; the second line shows prediction for each residue to be exposed or buried; the third line shows prediction of disorder. In *B* and *D*, 50–100 cells were quantified from three independent experiments. Error bars are 95% confidence interval. See also Supplementary Figure S1.

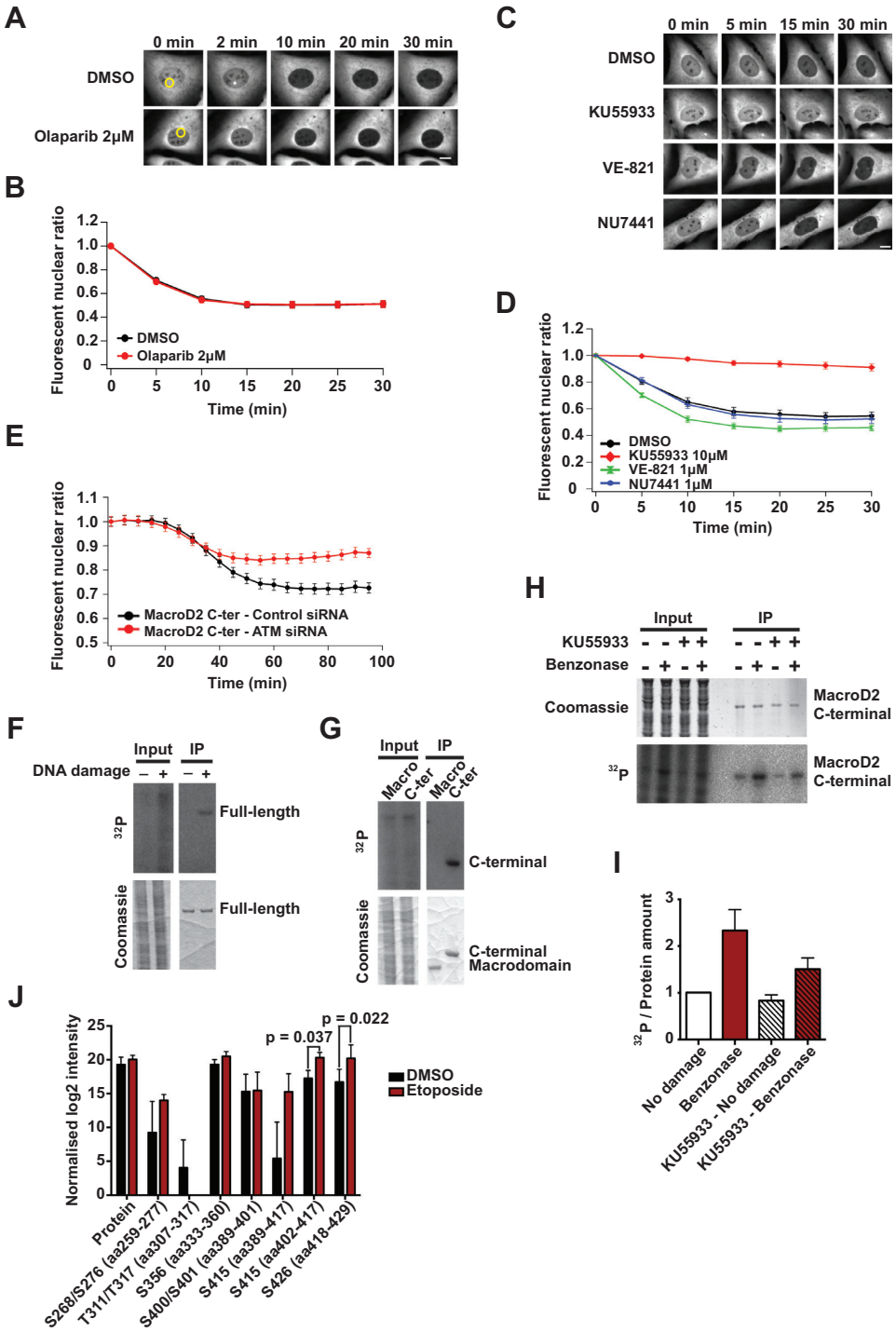

Figure 2. ATM kinase activity induces MacroD2 nuclear export. (**A**) Microirradiation live-cell microscopy of U2OS cells stably expressing mEGFP-MacroD2 full-length construct and treated with Olaparib 2 μM or DMSO. The focus of laser microirradiation is indicated with a yellow circle. Scale bar, 10 μm. (**B**) Quantification of *A*. (**C**) Microirradiation live-cell microscopy of U2OS cells stably expressing mEGFP-MacroD2 full-length construct and treated with KU55933 10 μM, VE-821 1 μM, NU7441 1 μM or DMSO. Scale bar, 10 μm. (**D**) Quantification of *C*. (**E**) Quantification of live-cell imaging experiments with U2OS cells stably expressing mYFP-MacroD2 C-terminal domain, pre-treated with siRNA against ATM or negative control siRNA for three days and treated with etoposide 10 μM. Error bars are 95% confidence interval. One representative experiment with more than 200 cells is shown. (**F**) Autoradiography and Coomassie staining of mEGFP-MacroD2 full-length protein purified from stably-expressing U2OS cell lysate, previously treated or not with benzonase and spiked with (^{32}P)γ-ATP. (**G**) Autoradiography and Coomassie staining of mEGFP-MacroD2 macrodomain or mEGFP-MacroD2 C-terminal region proteins immunopurified from stably-expressing U2OS cell lysates, previously treated with benzonase and spiked with (^{32}P)γ-ATP. (**H**) Coomassie and autoradiography of mEGFP-MacroD2 C-terminal domain added to HEK293 cell lysate, treated or not with benzonase and KU55933, spiked with (^{32}P)γ-ATP and successively immunopurified. (**I**) Quantification of *H* IP results in three independent experiments. Error bars, SEM. (**J**) Abundance of phosphorylated peptides of mEGFP-MacroD2 immunopurified from U2OS stably expressing the protein and treated with etoposide 10 μM or DMSO. Quantification of three independent experiments. Error bars, SEM. Statistics performed with paired t-Test with two-tailed distribution. In *B* and *D*, 50–100 cells were quantified from three independent experiments. Error bars are 95% confidence interval. See also Supplementary Table S1.

not involved in the process. Furthermore, the recruitment of MacroD2 to the sites of DNA damage does not facilitate or hinder its export from the nucleus. There are a number of other NAD^+ utilizing enzymes, among them several mono-ADP-ribosyl-transferases and sirtuins. To address if a reduction of NAD^+ levels affected MacroD2 nuclear export, we pre-treated U2OS cells expressing the mEGFP-tagged MacroD2 C-terminal fragment with FK866 to inhibit the activity of the NAMPT enzyme, and thus deplete the cellular NAD^+ pool (34,35). We did not observe any change in the DNA damage-induced nuclear export of the C-terminus of MacroD2 after NAMPT inhibition (Supplementary Figure S2A), further supporting the notion that MacroD2 is exported from the nucleus in a manner independent from the activity of PARPs and sirtuins.

The PI3K-related kinases—ATM, ATR and DNA-PK—play a pivotal role in the regulation of the DNA damage response (36). To address if any of the PIKK family members were responsible for the DNA damage-triggered MacroD2 export, we pre-treated U2OS cell expressing mEGFP-MacroD2 with specific inhibitors of ATM, ATR and DNA-PK, using KU55933, VE-821 and NU7441 respectively, and measured MacroD2 export following laser microirradiation (Figure 2C and D). The UV microirradiation induced MacroD2 export in the DMSO treated control, but the ATM inhibitor completely blocked the process. Neither ATR nor DNA-PK inhibitors reduced MacroD2 nuclear export. ATM inhibition also blocked MacroD2 export upon DNA damage induced by etoposide (Supplementary Figure S2B and C).

To further validate the role of ATM, we tested MacroD2 export after siRNA-mediated knockdown of ATM (Supplementary Figure S2D). The RNAi-mediated depletion of ATM reduced the export of both the C-terminal construct and full-length MacroD2 upon etoposide treatment (Figure 2E; Supplementary Figure S2E). The incomplete block of MacroD2 export in the ATM depleted cells could be due to either residual ATM activity or other kinases functionally redundant with ATM. To differentiate between these two possibilities, we measured the etoposide-induced export of the MacroD2 C-terminal IDR by combining ATM RNAi with small molecule inhibitors of ATM, ATR or DNA-PK (Supplementary Figure S2F). The combination of ATM RNAi treatment and ATM inhibitor successfully blocked the process. On the other hand, when ATR or DNA-PK inhibitors are combined with ATM RNAi treatment, MacroD2 exports as fast as the control DMSO. These results show that activation of ATM is necessary and sufficient for MacroD2 export upon DNA damage.

ATM activation leads to phosphorylation of the MacroD2 C-terminal region

Considering that ATM activation generates a cascade of phosphorylation events (15), we wanted to test if MacroD2 is phosphorylated upon DNA damage. By using $(^{32}P)\gamma$ ATP, we induced DNA damage by adding benzonase nuclease to the extract from U2OS cells stably expressing MacroD2 constructs (Figure 2F). No radioactivity was detected in case of the macrodomain-only construct, indicating that the C-terminal part of the protein is the primary target of the modification (Figure 2G). Also, when we incubated the purified mEGFP-tagged MacroD2 C-terminal-fragment in HEK293 lysate treated with benzonase nuclease, the radioactive signal of MacroD2 is decreased, if KU55933 is added to the reaction (Figure 2H and I).

To further confirm the DNA damage-induced phosphorylation of MacroD2, we adopted a mass-spectrometry-based phospho-proteomics approach measuring the abundance of phosphorylated peptides from MacroD2 in samples with or without etoposide treatment. Among a selection of peptides (70% sequence coverage), some sites in MacroD2 showed increased phosphorylation upon etoposide treatment as compared with control, like S415 and S426 (Figure 2J; Supplementary Table S1). In particular, the phosphorylated version of the peptide 402–417 is highly enriched upon etoposide treatment and, given the short size of the peptide and the absence of other compatible residues, the phosphorylation occurs at S415. Based on the mass-spectrometry data, we estimated that ∼14% of peptide 402–417 is phosphorylated upon etoposide treatment (Supplementary Table S1). Assuming that the ratio of the nuclear and cytoplasmic volumes is about 1:4 and that upon etoposide treatment around 60% of the nuclear MacroD2 remains in the nucleus, it means that only about 12% of the total pool of MacroD2 protein remains in the nucleus after DNA damage. The level of observed MacroD2 phosphorylation upon DNA damage would be consistent with MacroD2 being mostly present as phosphorylated on S415 in the nucleus where ATM kinase activity dominates while in the cytoplasm, S415 of MacroD2 is efficiently dephosphorylated and is predominantly in a non-phosphorylated state.

Sequence requirements for the phosphorylation are consistent with the direct involvement of ATM

The C-terminal region of MacroD2 is rich in serine and threonine residues, with four of the serines followed by glutamine (Figure 3A for a schematic view). The SQ/TQ motif is indeed a consensus target of ATM and other PIKK members (37). When we mutated all four serine residues within the SQ motifs to alanine (mutant 4SA), MacroD2 nuclear export upon DNA damage was blocked (Figure 3B and C). To address the specific contribution of each motif to nuclear export, we created four mutants, each with three of the four serines mutated to alanine, leaving only one SQ motif intact per construct (Figure 3D; Supplementary Figure S3A). We found both S345 and S415 alone to be sufficient for MacroD2 nuclear export, even though their export rate did not reach that of wild type, indicating that the two regions act co-operatively.

We sought to further characterize the importance of residues in the export-competent region. We decided to focus on serine 415, since this serine was the best characterized in our phospho-proteomics analysis. We tested a series of fragments with decreasing length to find a sequence short enough to be further manipulated but still able to export (Supplementary Figure S3B and C). We found that the 9-residue-long fragment between amino acids 410–418 showed strongly reduced, yet measurable export. Next, we addressed to what extent each residue in this sequence is required for phosphorylation. To this end, we adopted a scan-

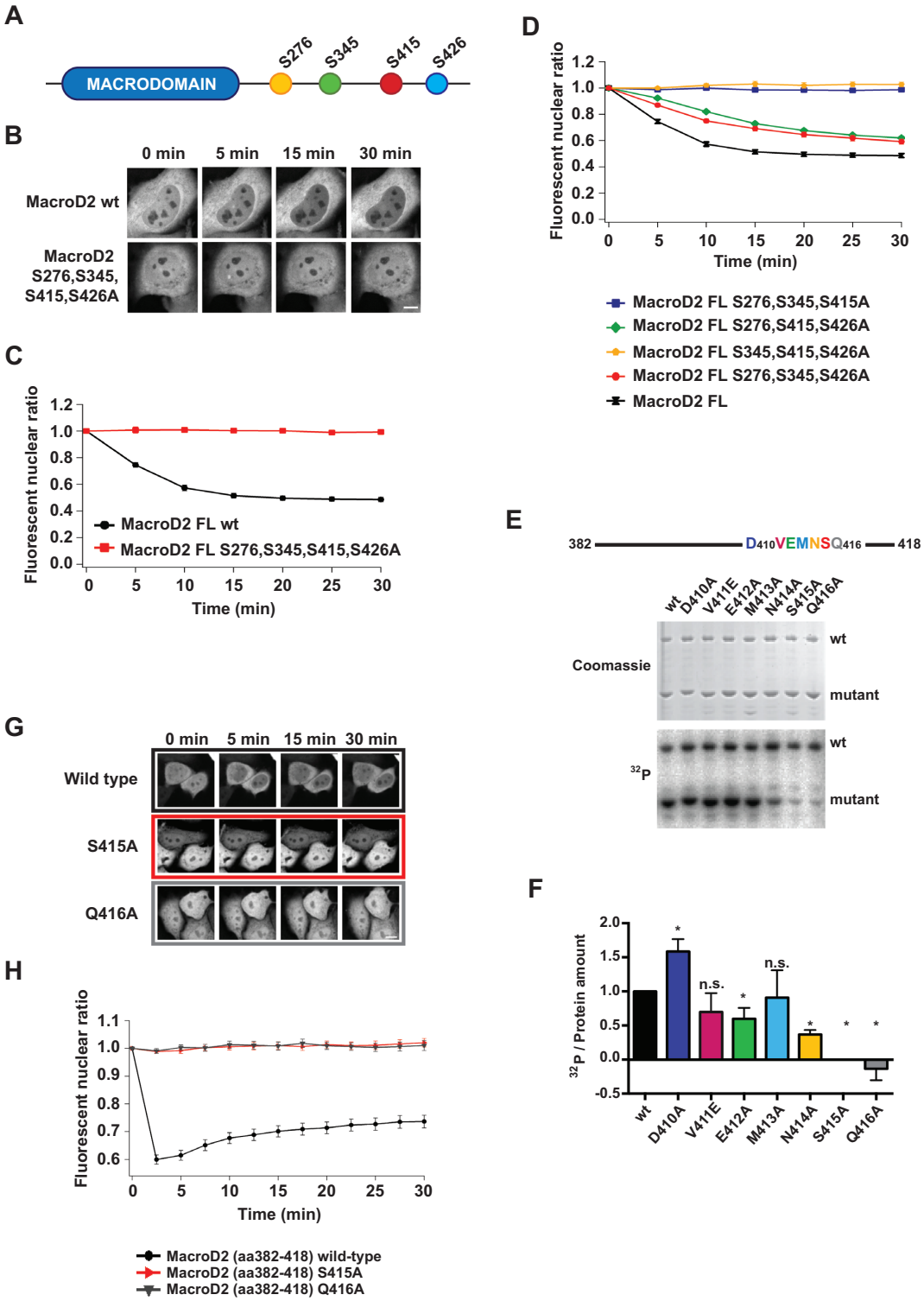

Figure 3. Sequence requirements for the phosphorylation are consistent with the direct involvement of ATM. (**A**) Schematic view showing the four SQ motifs present on the C-terminal domain. (**B**) Microirradiation live-cell microscopy of HeLa cells transfected with mEGFP-MacroD2 full-length or mEGFP-MacroD2 S276,345,415,426A constructs. Scale bar, 10 μm. (**C**) Quantification of *B*. (**D**) Quantification of microirradiation live-cell microscopy of HeLa cells transfected with mEGFP-MacroD2 full length or the different serine triple mutants (Examples shown in Supplementary Figure S3A). (**E**) Coomassie and autoradiography of GST-mEGFP-MacroD2 (aa382–418) wild-type and His-mEGFP-MacroD2 (aa382–418) (wild-type or mutant proteins) immunopurified from HEK293 cell lysate, treated with benzonase and spiked with (^{32}P)γ-ATP. (**F**) Quantification of *E* in three independent experiments. Error bars, SEM. Statistics performed with unpaired non-parametrical Mann-Whitney test against the wild-type. *$P \leq 0.05$; n.s. is $P > 0.05$. (**G**) Microirradiation live-cell microscopy of HeLa cells transfected with mEGFP-MacroD2 (aa382–418) wild-type construct or mutations of S415A or Q416A. Scale bar, 10 μm. (**H**) Quantification of *G*. In *C*, *D* and *G*, 50–100 cells were quantified from three independent experiments. Error bars are 95% confidence interval. See also Supplementary Figure S3.

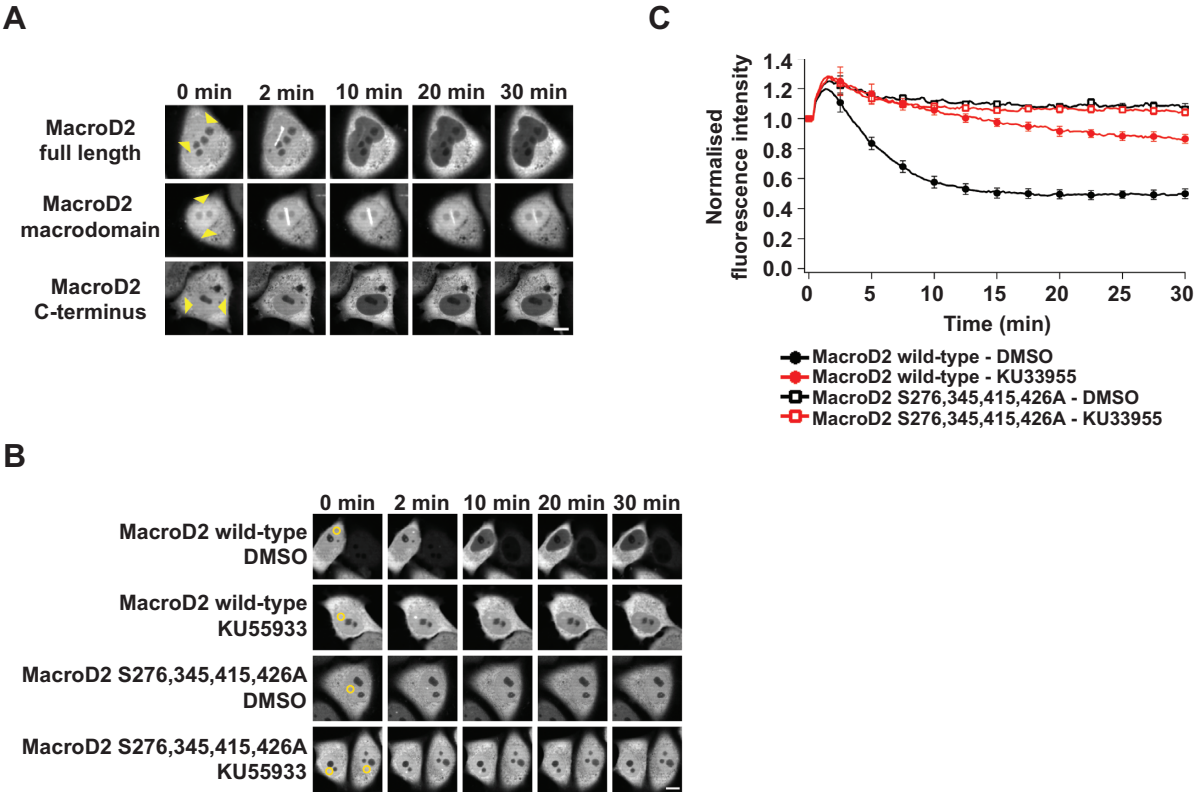

Figure 4. ATM activity regulates the recruitment of MacroD2 to sites of DNA damage. (**A**) Recruitment of tagged mEGFP-MacroD2 constructs (full length, macrodomain or C-terminal domain) in HeLa cells. The focus of laser micro-irradiation is indicated with yellow arrowheads. Scale bar, 10 μm. (**B**) Recruitment of tagged mEGFP-MacroD2 constructs (wild-type or S276 345 415 426A mutant) in HeLa cells. The focus of laser micro-irradiation is indicated with a yellow circle. Scale bar, 10 μm. (**C**) Quantification of *B* performed on 15 cells from three independent experiments. Error bars are 95% confidence interval.

ning mutagenesis approach, mutating each residue of the 410–416 stretch to alanine (or aspartate in the case of V411) within the mEGFP-MacroD2 (382–418) fragment. To assay the kinase activity, we used HEK293 cell lysates spiked with the purified proteins and treated with benzonase nuclease. We tested the incorporation of (^{32}P)-phosphate in the His-mEGFP-tagged mutagenized fragments compared to the GST-mEGFP-tagged wild-type fragment, which acted as an internal positive control for phosphorylation (Figure 3E and F). We confirmed that the mutations of either S415 or Q416 impair the phosphorylation of the fragments. Finally, we tested the mutation of S415 or Q416 with a mEGFP-tag in export assays upon UV microirradiation (Figure 3G and H). Significantly, both S415 and Q416 are necessary for nuclear export, which is also the case for S345 and Q346 (Supplementary Figure S3D). Our experiments reveal that two of the four SQ motifs in the C-terminal IDR are crucial for MacroD2 nuclear export and appear to work in an additive manner. The observation that both the serine and the glutamine are crucial for both the phosphorylation and the export of MacroD2, strongly suggests that MacroD2 is a direct target of ATM kinase.

ATM activity regulates the recruitment of MacroD2 to sites of DNA damage

Lastly, we addressed if the ATM-induced MacroD2 nuclear export could affect MacroD2 recruitment to sites of DNA damage. We compared the recruitment dynamics of mEGFP-tagged MacroD2 full-length, MacroD2 macrodomain and MacroD2 C-terminus proteins upon UV microirradiation (Figure 4A). Both MacroD2 full-length and macrodomain recruited to DNA damage sites, while the mEGFP-MacroD2 C-terminus fragment did not. But recruitment at the DNA lesion differs between MacroD2 full-length and MacroD2 macrodomain, since the full-length protein is dissipated faster than the macrodomain version. To assess whether MacroD2 nuclear export impacts on the recruitment dynamics, we compared the accumulation of EGFP-tagged wild type MacroD2 with that of the export-incompetent (4SA) mutant at the UV microirradiated sites, in the presence of the ATM inhibitor, KU55933, or DMSO control (Figure 4B and C). MacroD2 full-length recruitment peaked 2 min after laser irradiation. Afterwards, the protein amount at the sites of DNA damage—and within the whole nucleus—decreased, which led to the loss of MacroD2 proteins at the damage site within 5 min. Both ATM inhibition and export-abolishing mutations in MacroD2 resulted in longer retention of MacroD2 at the DNA damage sites: recruitment was detected until the

end of the experiment (30 minutes). These results suggest that nuclear ADP-ribosylation could be modulated upon DNA damage through the ATM-induced nuclear export of MacroD2.

DISCUSSION

We found that MacroD2 is exported from the nucleus upon DNA damage and that this depends on the ATM-induced phosphorylation of the MacroD2 C-terminal IDR. The export-inducing phosphorylation occurs on two serine residues, both followed by glutamine, and these SQ/TQ motifs are modified by the PI3K-like kinases (37). The observation that the glutamine after the serine is absolutely required for phosphorylation and consequently nuclear export suggests that MacroD2 is a direct target of ATM.

ATM kinase is involved in the initial steps of DNA damage signaling and coordinates different cellular pathways to achieve either cell survival or apoptosis (15). Among its many effects, ATM activation can induce changes in the subcellular localization of a number of proteins, either directly or indirectly, such as the NF-κB essential modulator, NEMO, or the p53-ubiquitin ligase COP1 (38,39). Likewise, ATM induces the regulation of MacroD2 localization. Still, the sequences surrounding MacroD2 SQ motifs differ from those previously described proteins, suggesting that the MacroD2 mode of export employs a different export mechanism.

Importantly, our findings indicate that the ATM-dependent MacroD2 nuclear export creates an additional regulatory node between ATM signaling and ADP-ribosylation upon DNA damage. In recent years, several factors involved in homology-driven repair and ATM signaling – among them ATM itself – have been shown to recruit to DNA breaks thanks to PAR-binding motifs (2). For example, NBS1 and MRE11 recruitment depends on PARP1 activation, and the formation of the MRE11-RAD50-NBS1 (MRN) complex is pivotal for ATM activation (40). Due to ATM-induced MacroD2 nuclear export, MacroD2 is cleared faster from the sites of DNA damage as compared to without export, suggesting that ATM activation alters ADP-ribosylation dynamics. The role of ATM in the clearance of MacroD2 from DNA lesions might be linked with the oncogenic features recently associated to MacroD2, where MacroD2 is found to be over-expressed in tamoxifen-resistant and estrogen-independently growing breast cancer cell lines (21). Thus, how the nuclear export of MacroD2 modulates the ADP-ribosylated proteins, and consequently the DNA damage response, will be the next important step in understanding the underlying molecular mechanisms of this novel crosstalk between two crucial DNA damage-induced signalling pathways.

SUPPLEMENTARY DATA

Supplementary Data are available at NAR Online.

ACKNOWLEDGEMENTS

We thank E. Kremmer for the anti-GAPDH antibody (Helmholtz Zentrum Munich), C. Riske of the Animal facility, A. Bowman, A.G. Ladurner, A.P. Nardozza and R. Smith for discussions, A.G. Ladurner and C. Laverty for comments on the manuscript.

FUNDING

Ludwig-Maximilians-Universität München (to G.T.); Deutsche Forschungsgemeinschaft [TI 817/2-1 to G.T.]; B.G. was supported by EU FP7 Marie Curie Initial Training Network 'Nucleosome4D' (granted through A.G. Ladurner). Funding for open access charge: Deutsche Forschungsgemeinschaft.
Conflict of interest statement. None declared.

REFERENCES

1. Caldecott,K.W. (2014) Protein ADP-ribosylation and the cellular response to DNA strand breaks. *DNA Repair*, **19**, 108–113.
2. Golia,B., Singh,H.R. and Timinszky,G. (2015) Poly-ADP-ribosylation signaling during DNA damage repair. *Front. Biosci.*, **20**, 440–457.
3. Ryu,K.W., Kim,D.S. and Kraus,W.L. (2015) New facets in the regulation of gene expression by ADP-ribosylation and poly(ADP-ribose) polymerases. *Chem. Rev.*, **115**, 2453–2481.
4. Hottiger,M.O., Hassa,P.O., Luscher,B., Schuler,H. and Koch-Nolte,F. (2010) Toward a unified nomenclature for mammalian ADP-ribosyltransferases. *Trends Biochem. Sci.*, **35**, 208–219.
5. Butepage,M., Eckei,L., Verheugd,P. and Luscher,B. (2015) Intracellular Mono-ADP-Ribosylation in signaling and disease. *Cells*, **4**, 569–595.
6. Tanny,J.C., Dowd,G.J., Huang,J., Hilz,H. and Moazed,D. (1999) An enzymatic activity in the yeast Sir2 protein that is essential for gene silencing. *Cell*, **99**, 735–745.
7. Haigis,M.C., Mostoslavsky,R., Haigis,K.M., Fahie,K., Christodoulou,D.C., Murphy,A.J., Valenzuela,D.M., Yancopoulos,G.D., Karow,M., Blander,G. *et al.* (2006) SIRT4 inhibits glutamate dehydrogenase and opposes the effects of calorie restriction in pancreatic beta cells. *Cell*, **126**, 941–954.
8. Liszt,G., Ford,E., Kurtev,M. and Guarente,L. (2005) Mouse Sir2 homolog SIRT6 is a nuclear ADP-ribosyltransferase. *J. Biol. Chem.*, **280**, 21313–21320.
9. Kassner,I., Andersson,A., Fey,M., Tomas,M., Ferrando-May,E. and Hottiger,M.O. (2013) SET7/9-dependent methylation of ARTD1 at K508 stimulates poly-ADP-ribose formation after oxidative stress. *Open Biol.*, **3**, 120173.
10. Mao,Z., Hine,C., Tian,X., Van Meter,M., Au,M., Vaidya,A., Seluanov,A. and Gorbunova,V. (2011) SIRT6 promotes DNA repair under stress by activating PARP1. *Science*, **332**, 1443–1446.
11. Wright,R.H., Castellano,G., Bonet,J., Le Dily,F., Font-Mateu,J., Ballare,C., Nacht,A.S., Soronellas,D., Oliva,B. and Beato,M. (2012) CDK2-dependent activation of PARP-1 is required for hormonal gene regulation in breast cancer cells. *Genes Dev.*, **26**, 1972–1983.
12. Matsuoka,S., Ballif,B.A., Smogorzewska,A., McDonald,E.R. 3rd, Hurov,K.E., Luo,J., Bakalarski,C.E., Zhao,Z., Solimini,N., Lerenthal,Y. *et al.* (2007) ATM and ATR substrate analysis reveals extensive protein networks responsive to DNA damage. *Science*, **316**, 1160–1166.
13. Gagne,J.P., Moreel,X., Gagne,P., Labelle,Y., Droit,A., Chevalier-Pare,M., Bourassa,S., McDonald,D., Hendzel,M.J., Prigent,C. *et al.* (2009) Proteomic investigation of phosphorylation sites in poly(ADP-ribose) polymerase-1 and poly(ADP-ribose) glycohydrolase. *J. Proteome Res.*, **8**, 1014–1029.
14. Bensimon,A., Schmidt,A., Ziv,Y., Elkon,R., Wang,S.Y., Chen,D.J., Aebersold,R. and Shiloh,Y. (2010) ATM-dependent and -independent dynamics of the nuclear phosphoproteome after DNA damage. *Sci. Signal.*, **3**, rs3.
15. Shiloh,Y. and Ziv,Y. (2013) The ATM protein kinase: regulating the cellular response to genotoxic stress, and more. *Nat. Rev. Mol. Cell Biol.*, **14**, 197–210.
16. Haince,J.F., Kozlov,S., Dawson,V.L., Dawson,T.M., Hendzel,M.J., Lavin,M.F. and Poirier,G.G. (2007) Ataxia telangiectasia mutated (ATM) signaling network is modulated by a novel

poly(ADP-ribose)-dependent pathway in the early response to DNA-damaging agents. *J. Biol. Chem.*, **282**, 16441–16453.
17. Jankevicius,G., Hassler,M., Golia,B., Rybin,V., Zacharias,M., Timinszky,G. and Ladurner,A.G. (2013) A family of macrodomain proteins reverses cellular mono-ADP-ribosylation. *Nat. Struct. Mol. Biol.*, **20**, 508–514.
18. Rosenthal,F., Feijs,K.L., Frugier,E., Bonalli,M., Forst,A.H., Imhof,R., Winkler,H.C., Fischer,D., Caflisch,A., Hassa,P.O. *et al.* (2013) Macrodomain-containing proteins are new mono-ADP-ribosylhydrolases. *Nat. Struct. Mol. Biol.*, **20**, 502–507.
19. Sharifi,R., Morra,R., Appel,C.D., Tallis,M., Chioza,B., Jankevicius,G., Simpson,M.A., Matic,I., Ozkan,E., Golia,B. *et al.* (2013) Deficiency of terminal ADP-ribose protein glycohydrolase TARG1/C6orf130 in neurodegenerative disease. *EMBO J.*, **32**, 1225–1237.
20. Neuvonen,M. and Ahola,T. (2009) Differential activities of cellular and viral macro domain proteins in binding of ADP-ribose metabolites. *J. Mol. Biol.*, **385**, 212–225.
21. Mohseni,M., Cidado,J., Croessmann,S., Cravero,K., Cimino-Mathews,A., Wong,H.Y., Scharpf,R., Zabransky,D.J., Abukhdeir,A.M., Garay,J.P. *et al.* (2014) MACROD2 overexpression mediates estrogen independent growth and tamoxifen resistance in breast cancers. *Proc. Natl. Acad. Sci. U.S.A.*, **111**, 17606–17611.
22. Linnebacher,M., Ostwald,C., Koczan,D., Salem,T., Schneider,B., Krohn,M., Ernst,M. and Prall,F. (2013) Single nucleotide polymorphism array analysis of microsatellite-stable, diploid/near-diploid colorectal carcinomas without the CpG island methylator phenotype. *Oncol. Lett.*, **5**, 173–178.
23. van den Broek,E., Dijkstra,M.J., Krijgsman,O., Sie,D., Haan,J.C., Traets,J.J., van de Wiel,M.A., Nagtegaal,I.D., Punt,C.J., Carvalho,B. *et al.* (2015) High prevalence and clinical relevance of genes affected by chromosomal breaks in colorectal cancer. *PLoS One*, **10**, e0138141.
24. Briffa,R., Um,I., Faratian,D., Zhou,Y., Turnbull,A.K., Langdon,S.P. and Harrison,D.J. (2015) Multi-Scale genomic, transcriptomic and proteomic analysis of colorectal cancer cell lines to identify novel biomarkers. *PLoS One*, **10**, e0144708.
25. Anney,R., Klei,L., Pinto,D., Regan,R., Conroy,J., Magalhaes,T.R., Correia,C., Abrahams,B.S., Sykes,N., Pagnamenta,A.T. *et al.* (2010) A genome-wide scan for common alleles affecting risk for autism. *Hum. Mol. Genet.*, **19**, 4072–4082.
26. Tsang,K.M., Croen,L.A., Torres,A.R., Kharrazi,M., Delorenze,G.N., Windham,G.C., Yoshida,C.K., Zerbo,O. and Weiss,L.A. (2013) A genome-wide survey of transgenerational genetic effects in autism. *PloS One*, **8**, e76978.
27. Jones,R.M., Cadby,G., Blangero,J., Abraham,L.J., Whitehouse,A.J. and Moses,E.K. (2014) MACROD2 gene associated with autistic-like traits in a general population sample. *Psychiatric Gen.*, **24**, 241–248.
28. Hanai,S., Kanai,M., Ohashi,S., Okamoto,K., Yamada,M., Takahashi,H. and Miwa,M. (2004) Loss of poly(ADP-ribose) glycohydrolase causes progressive neurodegeneration in drosophila melanogaster. *Proc. Natl. Acad. Sci. U.S.A.*, **101**, 82–86.
29. Timinszky,G., Till,S., Hassa,P.O., Hothorn,M., Kustatscher,G., Nijmeijer,B., Colombelli,J., Altmeyer,M., Stelzer,E.H., Scheffzek,K. *et al.* (2009) A macrodomain-containing histone rearranges chromatin upon sensing PARP1 activation. *Nat. Struct. Mol. Biol.*, **16**, 923–929.
30. Kamentsky,L., Jones,T.R., Fraser,A., Bray,M.A., Logan,D.J., Madden,K.L., Ljosa,V., Rueden,C., Eliceiri,K.W. and Carpenter,A.E. (2011) Improved structure, function and compatibility for CellProfiler: modular high-throughput image analysis software. *Bioinformatics (Oxford, England)*, **27**, 1179–1180.
31. Jensen,S.S. and Larsen,M.R. (2007) Evaluation of the impact of some experimental procedures on different phosphopeptide enrichment techniques. *Rapid Commu. Mass Spectrom.: RCM*, **21**, 3635–3645.
32. Vizcaíno,J.A., Deutsch,E.W., Wang,R., Csordas,A., Reisinger,F., Ríos,D., Dianes,J.A., Sun,Z., Farrah,T., Bandeira,N. *et al.* (2014) ProteomeXchange provides globally coordinated proteomics data submission and dissemination. *Nat. Biotechnol.*, **32**, 223–226.
33. Rost,B., Yachdav,G. and Liu,J. (2004) The PredictProtein server. *Nucleic Acids Res.*, **32**, W321–W326.
34. Hasmann,M. and Schemainda,I. (2003) FK866, a highly specific noncompetitive inhibitor of nicotinamide phosphoribosyltransferase, represents a novel mechanism for induction of tumor cell apoptosis. *Cancer Res.*, **63**, 7436–7442.
35. Cambronne,X.A., Stewart,M.L., Kim,D., Jones-Brunette,A.M., Morgan,R.K., Farrens,D.L., Cohen,M.S. and Goodman,R.H. (2016) Biosensor reveals multiple sources for mitochondrial NAD(+). *Science (New York, N.Y.)*, **352**, 1474–1477.
36. Furgason,J.M. and Bahassi el,M. (2013) Targeting DNA repair mechanisms in cancer. *Pharmacol. Ther.*, **137**, 298–308.
37. Kim,S.T., Lim,D.S., Canman,C.E. and Kastan,M.B. (1999) Substrate specificities and identification of putative substrates of ATM kinase family members. *J. Biol. Chem.*, **274**, 37538–37543.
38. Wu,Z.H., Shi,Y., Tibbetts,R.S. and Miyamoto,S. (2006) Molecular linkage between the kinase ATM and NF-kappaB signaling in response to genotoxic stimuli. *Science (New York, N.Y.)*, **311**, 1141–1146.
39. Su,C.H., Zhao,R., Velazquez-Torres,G., Chen,J., Gully,C., Yeung,S.C. and Lee,M.H. (2010) Nuclear export regulation of COP1 by 14-3-3sigma in response to DNA damage. *Mol. Cancer*, **9**, 243.
40. Haince,J.F., McDonald,D., Rodrigue,A., Dery,U., Masson,J.Y., Hendzel,M.J. and Poirier,G.G. (2008) PARP1-dependent kinetics of recruitment of MRE11 and NBS1 proteins to multiple DNA damage sites. *J. Biol. Chem.*, **283**, 1197–1208.